J. Phys. B: At. Mol. Opt. Phys. 28 (1995) 445–456. Printed in the UK

Partial and total cross sections for single electron capture by Ar^{8+} from He in the 400–2400 eV energy range

A Gosselin†, D Hennecart†, X Husson†‖, H Kucal†‖, D Leclerf†, A Lepoutre†, A Cassimi‡, J P Grandin‡, P Jardin‡ and C Adjouri§

† Laboratoire de Spectroscopie Atomique-ISMRA, 6 Boulevard Maréchal Juin, F-14050 Caen Cedex, France

‡ Ciril, Laboratoire commun du CEA et du CNRS rue Claude BLOCH BP 5133, F-14040 Caen Cedex, France

§ Laboratoire des Collisions Atomiques et Moléculaires Bâtiment 351, Université de Paris Sud, F-91405 Orsay Cedex, France

Received 15 July 1994, in final form 10 November 1994

Abstract. Charge-exchange processes in 400–2400 eV Ar^{8+}–He collisions are investigated: high energy resolution ion beam spectroscopy is performed with a recoil ion source (RIS) built in GANIL, total and partial cross sections for single-electron capture are measured using retarding field and energy gain techniques. Comparison with previous experimental results for total charge-exchange cross sections shows a rather good agreement and confirms the independence of these cross sections on the collision energy in the studied range. In contrast partial charge-exchange cross sections are shown to depend strongly on the collision energy. The experimental data are compared with theoretical results in the semi-classical impact parameter frame and with predictions made by other authors using the Landau–Zener model.

Introduction

Measurements of total and partial cross sections for charge-exchange processes between a multicharged A^{q+} ion and a neutral target B atom, in the very low collision energy range ($E \ll 1q$ keV) are of great interest. They provide tests for theoretical models of collision processes and useful data for astrophysics (Dalgarno and Butler 1978, Dalgarno 1985) and plasma-physics diagnostics (Joachain and Post 1983).

Up to now however, only few experimental results have been reported in this energy range. They were mainly obtained by the ion projectile translation spectroscopy technique which requires a very good energy definition for the incoming ion beam. Recoil ion sources (RIS) are well suited devices for the production of such beams (Cocke and Olson 1991). For this reason most of the low energy collision experiments made use of such recoil ion sources (Biederman *et al* 1990, Nielsen *et al* 1984, Cocke 1989). However it has been shown more recently that electron beam ion sources (EBIS) also provide beams with a comparable quality (Vancura *et al* 1992, Said *et al* 1992).

‖ Also at the University of Caen, UFR Sciences, France.

0953-4075/95/030445+12$19.50

We have built in our laboratories a recoil ion source and tested it at GANIL¶ (Gosselin 1993, Gosselin *et al* 1994).

This paper reports the first results which concern single capture experiments for the (Ar^{8+}-He) system in the 400–2400 eV collision energy range obtained with this source. We have measured total charge-exchange cross sections σ_{TOT}, using the retarding field method (Mann 1986). We have also determined partial charge-exchange cross sections, σ_{nl}, by energy gain spectrometry (Nielsen *et al* 1985).

In order to interpret our experimental results, semi-classical calculation of the collison is performed, based on the impact parameter approximation (IPM). Finally, we compare our results with the predictions of a Landau-Zener calculation due to Benmeuraien (1987a, b).

1. Experimental apparatus

Three parts can be distinguished in the experimental set-up which is shown in figure 1:

(A) *the recoil ion source* (RIS)

(B) the collision region

(C) the analyser (either energy gain spectrometer or retarding field analyser).

1.1. The recoil ion source

This RIS has been fully described by Gosselin (1993) and Gosselin *et al* (1994). We, nevertheless, recall here the main features. The incident ion beam (Kr^{31+}, 9 MeV A^{-1}, $I_p = 500$ nA) produced at the medium energy facility of GANIL (SME) crosses an argon gas cell and produces Ar recoil ions. A weak electric field which is produced between the electrodes biased at potentials V_1 and V_2, allows the extraction of the recoil ions from the production cell. These ions are then accelerated towards a Wien filter (WF) where charge-state selection is performed. The recoil ion beam of selected charge state q is then slowed down by the decelerating potential V_D. Two different Einzel lenses, L_1 before the WF, L_2 after the WF, and a set of deflecting plates are used to focus the beam on a 2 mm diameter aperture in the centre of the last electrode of the decelerating stage just before the collision region. More than 10^5 Ar^{8+} ions per second are obtained at this place in the recoil ion beam. The beam energy may easily be adjusted between 50 and 500 q eV with an energy dispersion lower than 0.5 q eV.

1.2. Collision region

The recoil ion beam interacts with a target consisting of a He supersonic gas jet J (Campargue 1984) in an equipotential region limited by two electrodes, 6 mm apart, biased at potential V_D. The second has in its centre a 20 mm diameter aperture covered by a 90% transmission nickel mesh. The He gas jet density is approximately 10^{13} atom/cm^3 and it has a diameter of about 2 mm in the collision region.

1.3. Analysers

1.3.1. Energy gain spectrometry. After the collision, the ions are energy analysed by a small parallel plate electrostatic deflector (ED). The distance between the two plates of

¶ Grand Accélérateur National d'Ions Lourds, Caen, France.

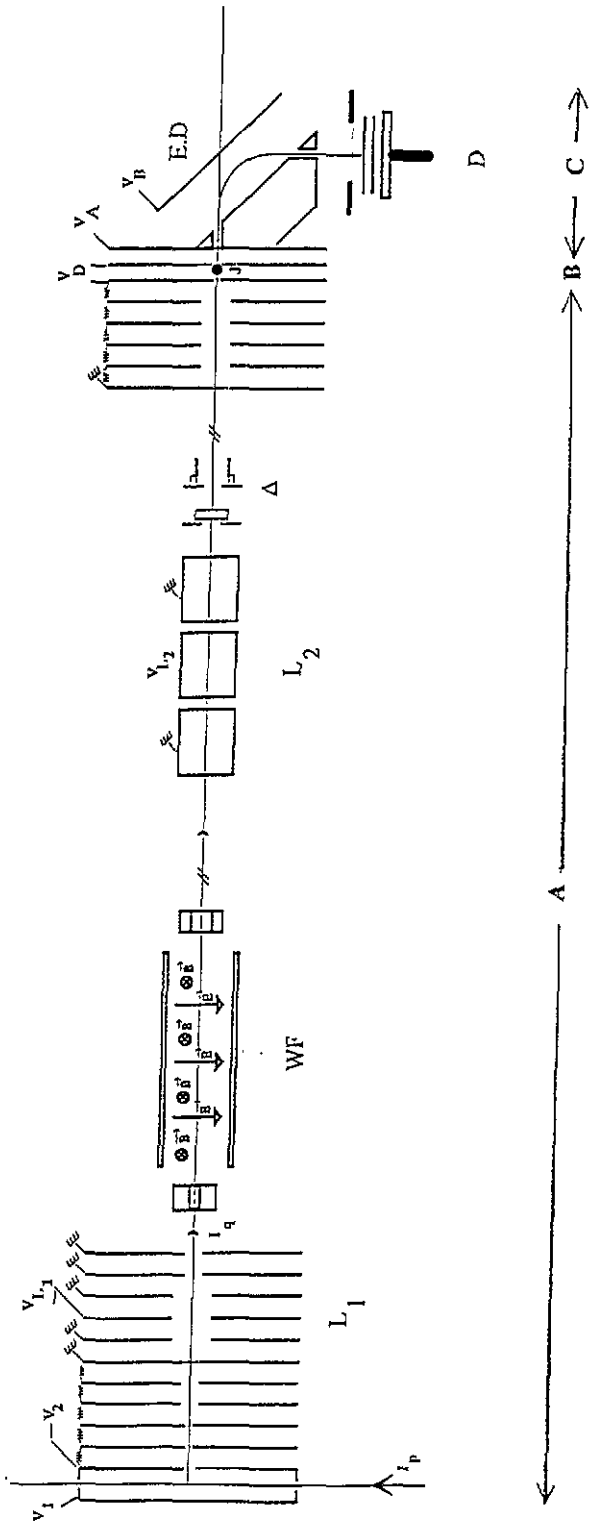

Figure 1. Experimental set-up; (A) the recoil ion source (RIS), (B) the collision region, (C) the analyser.

the deflector is 25 mm. The 1 mm wide input and output slits are separated by 50 mm. Satisfactory resolution is insured by a relatively small potential difference between the two plates ($V_A - V_B \cong 15$ V). The spectra are obtained by scanning the V_A voltage and recording the number of selected ions detected by a multichannel plate detector (D); the absolute resolution is about 0.5 q eV. The energy gain spectra provide identification of the electronic capture configurations (nl) and deduction of the corresponding partial cross sections σ_{nl} by a method which will be described hereafter.

1.3.2. Retarding field analysis. For the measurement of total charge-exchange cross sections, σ_{TOT}, a retarding field analyser (not represented in figure 1), similar to the decelerating stage placed before the collision region, was used in place of the parallel plate electrostatic deflector. By scanning the potential applied to this analyser, charge states q (incoming charge state), q_1, q_2 (respectively produced by one- and two-electron captures) may be successively reflected towards the source. Thus the spectra recorded on a detector placed behind the retarding field analyser display several steps, from the height of which the total cross sections σ_{TOT} may be deduced.

2. Results and discussion

2.1. Determination of electron capture configuration (nl)

Single electronic capture following the reaction:

$$Ar^{8+} + He \rightarrow (Ar^{7+})_{nl} + He^{+}(1s) + Q_{nl}$$

has been studied using the experimental set-up described previously. Here Q_{nl} is an energy defect which depends on the particular nl state into which the helium electron is captured.

During the collision the incident Ar^{8+} ions are deflected by an angle θ which cannot be neglected at such low energies. The measured energy gains will then depend on Q_{nl} and θ.

Five different energy defect spectra, recorded at 400, 560, 800, 1600 and 2400 eV collision energies, are shown in figure 2. Each of them exhibits two peaks.

From the positions and distances between these two peaks we can deduce the energy of the levels corresponding to simple electronic capture. From a comparison between these energies and the experimental Ar^{7+} energy levels (Moore 1949) we conclude that single electron capture populates 5p and 5s configurations (left peaks on figure 2) and 4f and 4d configurations (right peaks on figure 2). The resolution of our analyser does not allow separation of 5s from 5p contributions nor 4f from 4d. The expected positions of the peaks corresponding to the captures into these configurations for a zero degree scattering angle are also indicated by vertical lines on figure 2.

We observe that for decreasing collision energies:

(i) the intensity of the 5s–5p peak increases with regard to 4f–4d peak intensity;

(ii) the shift between the experimental and expected positions increases.

2.2. Determination of the most probable scattering angle

Using the equation of ion trajectories in the spectrometer (Gosselin 1993), the most probable scattering angle θ of Ar^{7+} may be deduced from the observed energy shifts.

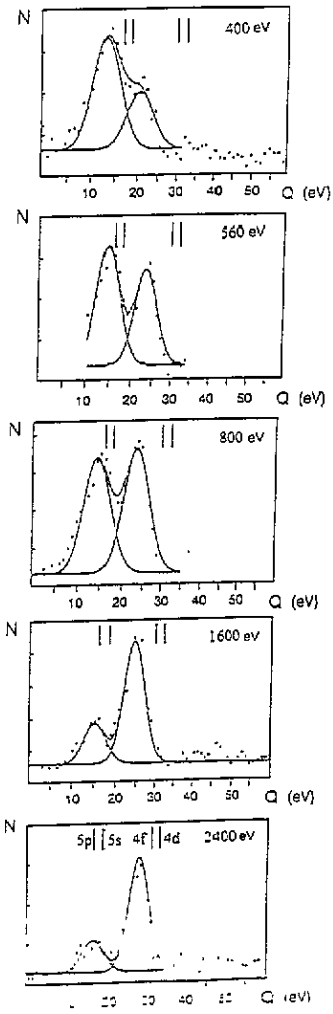

Figure 2. Energy defect spectra at different energies for Ar^{8+}–He simple capture collisions.

The values of θ calculated in this way are given in table 1. They were obtained according to two hypotheses for each peak: the first one corresponds to capture into either the 5p or 5s configurations and the second one to capture either into the 4f or 4d configurations. In each case it is observed that, as expected, θ increases for decreasing collision energies.

Table 1. Most probable scattering angle θ (in degrees) of Ar^{7+}, deduced from the experimental energy shift.

Energy (eV)	θ_{5p} (degrees)	θ_{5s} (degrees)	θ_{4f} (degrees)	θ_{4d} (degrees)
400	1.68	1.85	2.55	2.85
1600	0.57	0.75	0.90	1.15
2400	0.33	0.55	0.60	0.85

2.3. Determination of total σ_{TOT} and partial σ_{nl} capture cross sections

Let N_1 be the number of Ar^{8+} ions crossing the He target per second, N_2 the number of Ar^{7+} ions produced per second, d the density of the target and L the interaction length of the ion beam with the target. Then the total electronic capture cross section σ_{TOT} may be evaluated according to the following expression:

$$\sigma_{TOT} = \frac{N_2}{N_1 L d}.$$

In our experiments using the retarding field analyser, N_1 and N_2 may easily be obtained. In order to determine the Ld product we have performed another collision experiment on an Ar^{6+}–He system at 1800 eV energy for which the σ_{TOT} value has already been measured by Justiniano *et al* (1984). The 2 mm diameter diaphragm defining the Ar^{q+} ion beam (figure 1), as well as the use of a supersonic gas jet as a target, provide good definition reproducibility of the collision geometry used for Ar^{6+}–He and Ar^{8+}–He systems. The σ_{TOT} values deduced from these experiments for collision energies 800, 1600 and 2400 eV are presented on figure 3.

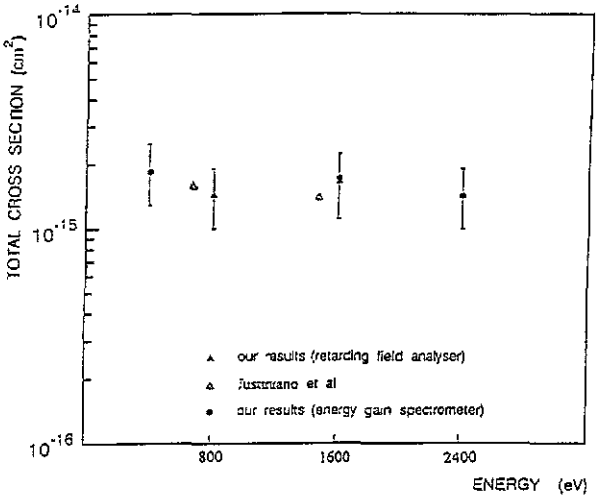

Figure 3. Comparison of total experimental cross sections σ_{TOT} for different collision energies; ▲, our results (retarding field analyser); △, Justiniano *et al* (1984); ●, our results (energy gain spectrometer).

From the area of the peaks observed on the energy-gain spectra, the partial cross sections σ_{nl} (and hence the total capture cross sections σ_{TOT} which are the sum of all the σ_{nl}) could be obtained provided that we could determine the detection loss of efficiency due to the angular scattering of the Ar^{7+} ions and to the limited angular acceptance of our analyser. In order to correct each peak area we have estimated (Gosselin 1993) a mean 'loss coefficient' using the equations of ion trajectories from the target to the detector and assuming for all the ions a scattering angle equal to the determined θ_{nl} values (at 1600 eV energy, for instance, only 80% of the ions having captured in 5s and 5p configurations and 60% of the ions having captured in 4d and 4f configurations are estimated to be detected). The corrected peak areas allow the σ_{nl} determination at different energies:

(i) at least for one energy collision we know the σ_{TOT} value previously measured (we choose the one obtained at 2400 eV by the retarding field method);

(ii) the acquisition conditions are comparable for all collision energies, which unfortunately was the case only for our experiments at 400, 1600 and 2400 eV.

We can observe on figure 3 that the σ_{TOT} obtained by the two methods are in very good agreement for collisions at 1600 eV. That *a posteriori* proves the correct evaluation of the 'loss coefficient' for which it is still difficult to evaluate the real uncertainty. The error bar (30%) plotted on the graph (figure 3) takes into account the 20% evaluated by Justiniano *et al* for the σ_{TOT} values for the Ar^{6+}–He system that we use as reference.

In figure 3 are also indicated the σ_{TOT} values obtained by Justiniano *et al* (1984) for the Ar^{8+}–He system at a collision energy close to ours. All these values are in good agreement and it is observed that σ_{TOT} values are rather independent of the value of the collision energy.

3. Semi-classical calculations

The calculations, that will be developed now, will serve to interpret the experimental results in the framework of the semi-classical molecular model. Examination of the energy-defect spectra suggests simple capture into Ar^{7+}(4d), Ar^{7+}(4f), Ar^{7+}(5s) and Ar^{7+}(5p) states (see section 3.1). However, the limited energy resolution does not allow one to unambiguously ascribe the peaks to a given state. In order to determine the individual contribution of each state, we have developed scattering close coupling calculations in the five states Ar^{7+}(4d), Ar^{7+}(4f), Ar^{7+}(5s), Ar^{7+}(5p) and He^{+}(1s) basis.

In this section diabatic potential calculations are presented, semi-classical transition probabilities are calculated in the impact parameter approximation (IPM). This collisional calculation will serve to describe single charge-exchange mechanisms in Ar^{8+} + He collisions which are involved at intermediate and large impact parameters. The results will be compared to Landau–Zener calculations (Benmeuraien 1987a, b) and to the experimental results.

3.1. Quasimolecular diabatic potentials and interactions in the PVB approach

The potentials and interactions are calculated in a *one-electron* PVB (projected valence bond) model (Kubach and Sidis 1981). This PVB model potential method has been successfully used to treat charge exchange of closed-shell ions such as B^{3+} with helium or neon target (Adjouri 1993, Adjouri *et al* 1994).

To describe the argon core orbitals, the Slater-type orbital (STO) basis set taken from Clementi (1965) is used; the STO $3l$, $4l$ and $5l$ are obtained as expansions of hydrogenic wavefunctions.

The interaction of the valence electron with the two $Ar^{8+} \equiv A$ and $He^{+} \equiv B$ ions is described by the model potentials:

$$V_A(r) = -\frac{q_A + \alpha_1 e^{-\beta_1 r}}{r}$$

and

$$V_B(r) = -\frac{q_B + \alpha_2 e^{-\beta_2 r}}{r}.$$

The charges $q_A = 8$ and $q_B = 1$ are those seen by the electron at large internuclear distance. The parameters $\alpha_1 = 19.1$ au, $\alpha_2 = 1$ au, $\beta_1 = 2.152$ au, $\beta_2 = 2.16$ au are adjusted to reproduce Ar^{7+} and He experimental binding energies.

Model potentials, multipolar interactions, coupling terms and electron charge-exchange interactions H_j (j: 4d, 4f, 5s, 5p) are calculated in the five ($1s_{He}$, $4d_{Ar}$, $4f_{Ar}$, $5s_{Ar}$, $5p_{Ar}$) PVB basis. The choice of minimal basis is stimulated by considering the experimental results. Having here *one-electron* calculations, the spin multiplicity is then considered in building the charge-exchange interactions. The exchange interactions H_j are easily obtained from the h_j one-electron interactions by:

$$H_{4d} = \sqrt{2}\, h_{4d} \qquad H_{4f} = \sqrt{2}\, h_{4f}$$

$$H_{5s} = \sqrt{2}\, h_{5s} \qquad H_{5p} = \sqrt{2}\, h_{5p}.$$

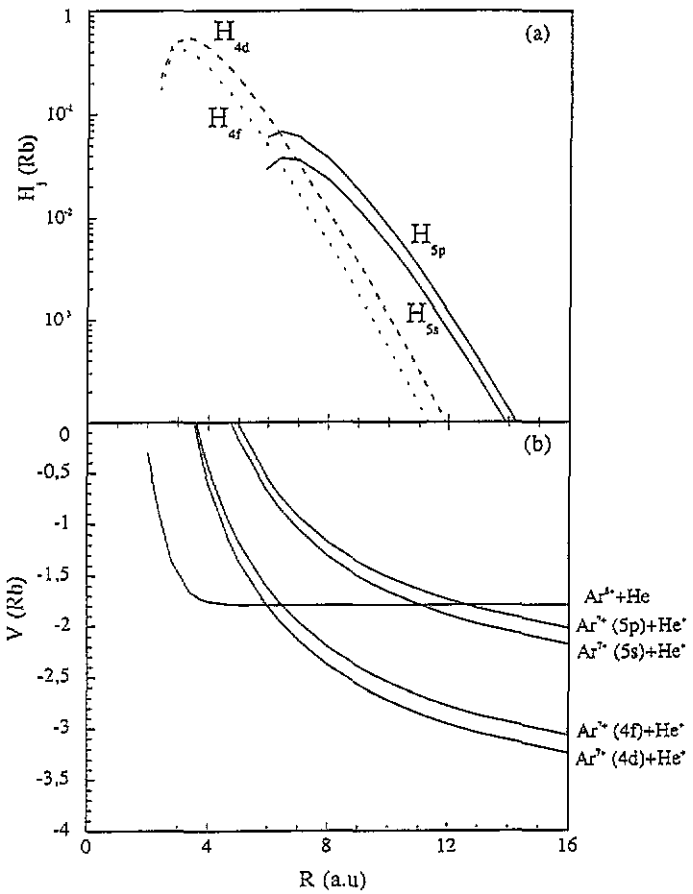

Figure 4. (*a*) Exchange interactions H_j (*j*: 4d, 4f, 5s and 5p) for the Ar^{8+}–He system for different values of the internuclear distance R. (*b*) Diabatic potential energy curves for the Ar^{8+}–He system.

An exponential behaviour of the exchange interactions H_j, figure 4(*a*), is found at moderate and large internuclear distances: justification of this kind of behaviour corresponding to the overlap of the wavefunctions has been given by Efremenkova *et al* (1974a, b). For comparison, the H_j values theoretically evaluated by Benmeuraien

(1987b) for the different crossing points are $H_{5s}=1.5\times10^{-3}$ au, $H_{4f}=9.5\times10^{-3}$ au, $H_{4d}=4.4\times10^{-2}$ au and $H_{4p}=8.5\times10^{-2}$ au.

To check the validity of the model potential method in the case of a helium target, previous calculations on the analogous B^{3+}–He system were performed (Adjouri 1993, Adjouri *et al* 1994). A good agreement with *ab initio* (Shipsey *et al* 1977) and other model potential calculations (Opradolce *et al* 1983) is found and gives us confidence in the application of the method to the $Ar^{8+}+He$ system.

Since the two initial Ar^{8+} and He states can only form singlet states and since singlet–triplet transitions via spin–orbit coupling from the initial singlet channel are assumed to be negligible, only singlet final states are considered. The $(ArHe)^{8+}$ diabatic molecular states are shown in figure 4(*b*). The interesting features are: (i) the two crossings between the entrance channel $Ar^{8+}+He$ 1Σ and the exit channels $Ar^{7+}(5s)+He^{+}$ and $Ar^{7+}(5p)+He^{+}$ around $R_{5s}\approx11$ au and $R_{5p}\approx12.5$ au, (ii) the inner crossings of the 1Σ with the exit channels associated to the 4d and 4f states around $R_{4d}\approx5.9$ au and $R_{4f}\approx6.4$ au respectively.

3.2. Single electron capture probabilities in 400–2400 eV Ar^{8+} + He collisions

We have developed a simple diabatic model for a qualitative understanding of the mechanisms responsible for the population of the different Ar^{7+} collisional states. We have solved the close-coupling equations for the five diabatic states in the impact parameter approximation using the PAMPA code (Gaussorgues *et al* 1965). The coupling terms

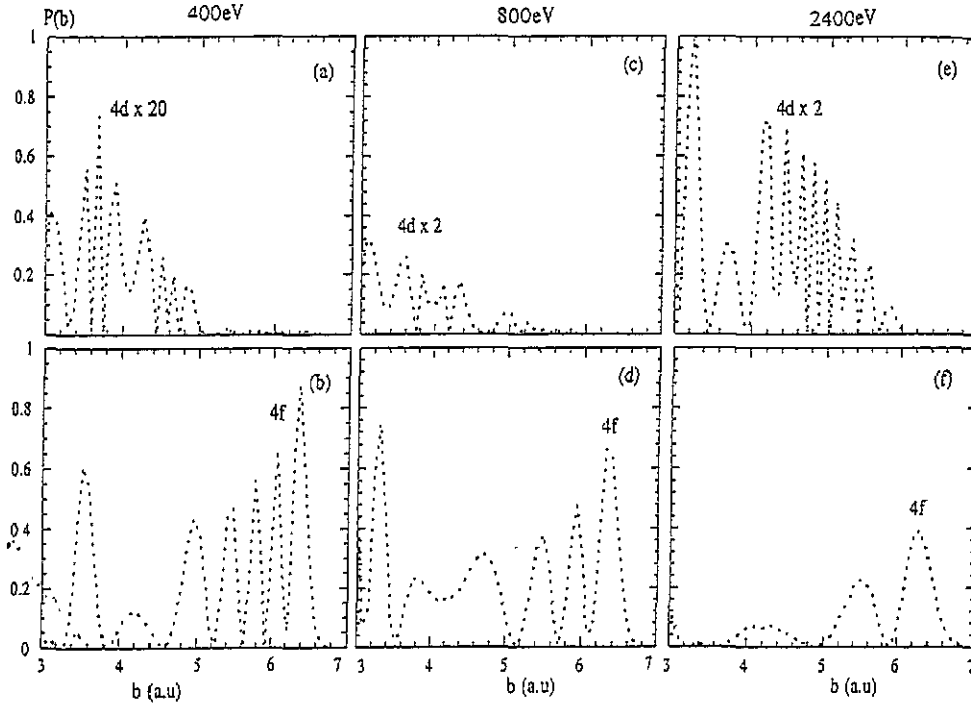

Figure 5. Capture probabilities into the Ar^{7+}(4d) and Ar^{7+}(4f) states as a function of impact parameter for $Ar^{8+}+He$ collision energies: (*a*) $E=400$ eV, (*b*) $E=800$ eV and (*c*) $E=2400$ eV.

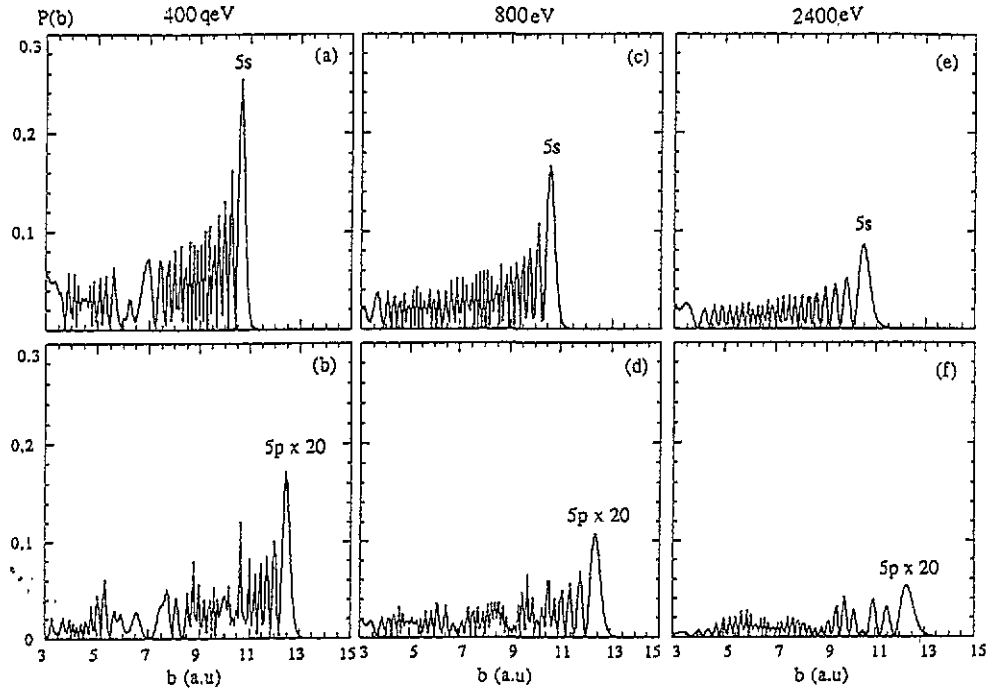

Figure 6. Capture probabilities into the $Ar^{7+}(5s)$ and $Ar^{7+}(5p)$ states as a function of impact parameter for $Ar^{8+}+He$ collision energies: (*a*) $E=400$ eV, (*b*) $E=800$ eV and (*c*) $E=2400$ eV.

and potential given above have been used. The rotational coupling term and electron translation factor (ETF) have been neglected since their effects are expected to be small at these low collision velocities. For each impact parameter b, the integration (Gaussorgues *et al* 1965) is performed in the interval $\pm z_{max}$ along the incident direction $z=vt$. The limit $z_{max}=20$ au is large enough to ensure that all considered couplings will vanish at this large distance.

The probabilities for single electron capture into $Ar^{7+}(4d)$, $Ar^{7+}(4f)$, $Ar^{7+}(5s)$ and $Ar^{7+}(5p)$ states as a function of impact parameter are shown in figures 5 and 6, in the 400–2400 q eV energy range. In the 5.9–6.5 au impact parameter range, clearly the $Ar^{7+}(4f)$ state population dominates and decreases with increasing energies in contrast to the $Ar^{7+}(4d)$ state. At large impact parameters, the transition probabilities in $Ar^{7+}(5s)$ and $Ar^{7+}(5p)$ states decrease with collision energy in agreement with the experimental behaviour (see figure 2). Integration of the transition probabilities over the impact parameter gives the total and partial cross sections (table 2). Examination of the σ_{4f} and σ_{4d} partial cross sections shows a clear evolution: in the 400–2400 eV energy range the σ_{4f} cross section dominates; above 1600 eV the σ_{4f} and σ_{4d} cross sections are nearly of the same order of magnitude. Concerning capture into $Ar^{7+}(5s)$ and $Ar^{7+}(5p)$ states, the σ_{5s}/σ_{5p} cross sections ratio is nearly equal to 20 in the 400–2400 eV energy range. We can conclude that the first peak observed in figure 2 corresponds chiefly to capture in the 5s level.

3.3. Experiment–theory comparisons

In figure 7, we compare the experimental $\sigma_{4d}+\sigma_{4f}$ and σ_{5s} partial cross sections with our five-states semi-classical results and the Landau–Zener calculations of Benmeuraien

Table 2. Partial cross sections for single electron capture determined by semi-classical calculations.

Collision Energy (eV)	σ_{5s} (10^{-16} cm^2)	σ_{5p} (10^{-16} cm^2)	σ_{4d} (10^{-16} cm^2)	σ_{4f} (10^{-16} cm^2)
400	5.29	0.24	0.20	7.95
560	4.52	0.20	0.50	8.41
800	3.83	0.17	1.07	7.81
1600	2.74	0.13	2.67	5.56
2400	2.31	0.10	3.75	3.74

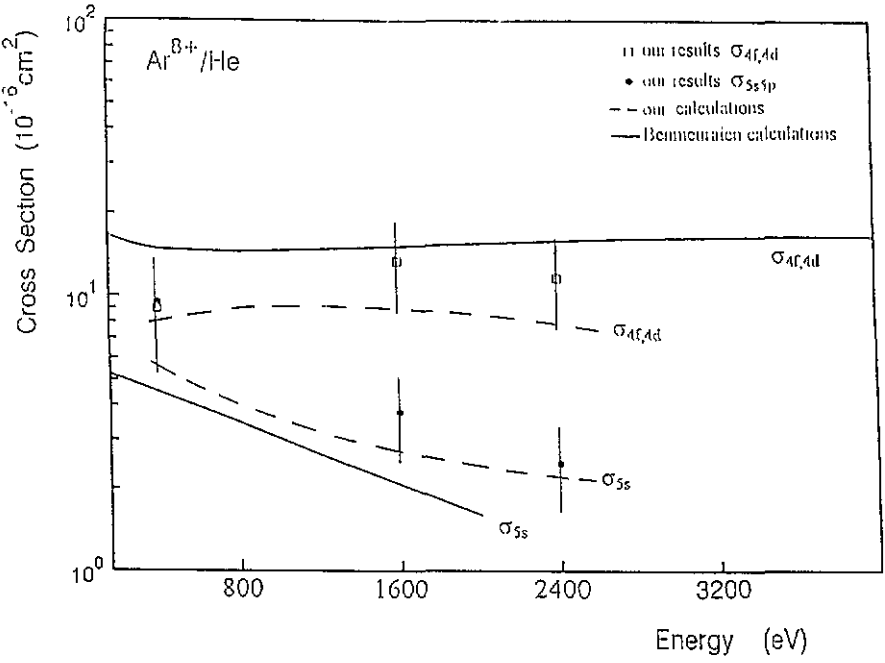

Figure 7. Partial cross sections (σ_{nl}) for electron capture by Ar^{8+} from He. Closed circles and open squares are the experimental σ_{nl} cross sections. Full lines represent the result of Benmeuraien (1987a, b) calculations. Dashed lines represent the result of our semi-classical calculations.

(1987a, b). We observe, for the σ_{5s} partial cross section, an agreement which is slightly better with our theoretical results than with Benmauraien's. The tendency of σ_{5s} to decrease when the collision energy increases is predicted by these two calculations and confirmed by the present experiment. For $\sigma_{4d} + \sigma_{4f}$ the agreement between experimental values and the two calculations is equivalent.

4. Conclusion

The use of a recoil ion source has allowed us to study the Ar^{8+}–He system in a low collision energy range. The measured total cross sections for charge exchange are in good agreement with previously obtained experimental values, their independence on the collision energy in the studied domain is confirmed. We have also shown that the

partial capture cross sections depend, in contrast, strongly on the collision energy. The experimental results are compared either to theoretical values obtained by Benmeuraien (1987a, b) using a Landau-Zener approach or to our semi-classical calculations. The latter leads to a better agreement, especially in the case of σ_{5s}.

Future work should concentrate on fully quantal calculations and take into account several outgoing channels and the different interactions responsible for transitions such as dielectronic interaction and rotational coupling.

References

Adjouri C 1993 *Thesis* Paris VI, unpublished

Adjouri C, Roncin P, Gaboriaud M N, Barat M and Andersen N 1994 *J. Phys. B: At. Mol. Opt. Phys.* **27** 3093

Benmeuraien L 1987a *Proc. 15th Int. Conf. on Physics of Electronic and Atomic Collisions (Brighton)* abstracts p 557

—— 1987b *Thesis* Bordaux unpublished

Biederman C, Cederquist H, Andersen L R, Levin J C, Short T, Elston S B, Gibbons J P, Anderson H, Liljeby L, and Sellin I A 1990 *Phys. Rev.* A **41** 5889

Campargue R 1984 *J. Phys. Chem.* **88** 4466

Clementi E 1965 Table of Atomic Functions *IBM J. Res. Dev.* **9** 2

Cocke C L 1989 *J. Physique Coll.* **C1** 19

Cocke C L and Olson R E 1991 *Phys. Rep.* **205** 155

Dalgarno A 1985 *Nucl. Instrum. Methods* **B9** 655

Dalgarno A and Butler S E 1978 *Comment. At. Mol. Phys.* 7 129

Efremenkova L Ya, Radsig A A and Smirnov B M 1974a *Opt. Spectrosk.* **36** 35

—— 1974b *Opt. Spectrosk.* **36** 61

Gaussorgues C, Piacentini R D and Salin A 1975 *Comput. Phys. Commun.* **10** 223

Gosselin A 1993 *Thesis* Caen (unpublished)

Gosselin A, Boduch P, Hennecart D, Hicham S, Husson X, Lecler D, Lepoutre A, Cassimi A and Grandin J P 1994 *J. Physique III* **4** 1765

Joachain C J and Post D E (ed) 1983 *Atomic and Molecular Processes in Controlled Thermonuclear Fusion* (New York: Plenum)

Justinaiano E, Cocke C L, Gray T J, Dubois R, Can C, Waggoner W, Schuch R, Schmidt-Böcking H and Ingwersen H 1984 *Phys. Rev.* A **29** 1088

Kuback C and Sidis V 1981 *Phys. Rev.* A **23** 110

Mann R 1986 *Z. Phys.* D **3** 85

Moore C E 1949 *Atomic energy levels* NBS Circular No 467, vol I (Washington, DC: US Govt. Printing Office) p224

Nielsen E H, Andersen L H, Barany A, Cederquist H, Heinemer J, Hvelplund P, Knudsen H and MacAdam K B 1985 *J. Phys. B: At. Mol. Phys.* **18** 1789

Nielson E H, Andersen L H, Barany A, Cederquist H, Hvelplund P, Knudsen H, MacAdam K B and Sorensen J 1984 *J. Phys. B: At. Mol. Phys.* **17** L139

Opradolce L, Valiron P and McCarroll 1983 *J. Phys. B: At. Mol. Phys.* **16** 2017

Said R, Kamber E Y, Yaltkaya S, gopinathan M and Ferguson S M 1992 *Proc. VIth HCI (Manhattan)* abstracts A 29

Shipsey E J, Browne J C and Olsen R E 1977 *Phys. Rev.* A **15** 2166

Vancura J and Kostroun V O 1992 *Proc. VIth HCI* (Manhattan) abstracts A 14